THE JOURNAL OF PHYSICAL CHEMISTRY B

pubs.acs.org/JPCB Article

The Laser-Induced Potential Jump: A Method for Rapid Electron Injection into Oxidoreductase Enzymes

Monica L. K. Sanchez, Sara E. Konecny, Sarah M. Narehood, Edward J. Reijerse, Wolfgang Lubitz, James A. Birrell,* and R. Brian Dyer*

Cite This: https://dx.doi.org/10.1021/acs.jpcb.0c05718 Read Online

ACCESS | Metrics & More | Article Recommendations | Supporting Information

ABSTRACT: Oxidoreductase enzymes often perform technologically useful chemical transformations using abundant metal cofactors with high efficiency under ambient conditions. The understanding of the catalytic mechanism of these enzymes is, however, highly dependent on the availability of well-characterized and optimized time-resolved analytical techniques. We have developed an approach for rapidly injecting electrons into a catalytic system using a photoactivated nanomaterial in combination with a range of redox mediators to produce a potential jump in solution, which then initiates turnover via electron transfer (ET) to the catalyst. The ET events at the nanomaterial-mediator-catalyst interfaces are, however, highly sensitive to the experimental conditions such as photon flux, relative concentrations of system components, and pH. Here, we present a systematic optimization of these experimental parameters for a specific catalytic system, namely, [FeFe] hydrogenase from *Chlamydomonas reinhardtii* (*Cr*HydA1). The developed strategies can, however, be applied in the study of a wide variety of oxidoreductase enzymes. Our potential jump system consists of CdSe/CdS core−shell nanorods as a photosensitizer and a series of substituted bipyridinium salts as mediators with redox potentials in the range from −550 to −670 mV (vs SHE). With these components, we screened the effect of pH, mediator concentration, protein concentration, photosensitizer concentration, and photon flux on steady-state photoreduction and hydrogen production as well as ET and potential jump efficiency. By manipulating these experimental conditions, we show the potential of simple modifications to improve the tunability of the potential jump for application to study oxidoreductases.

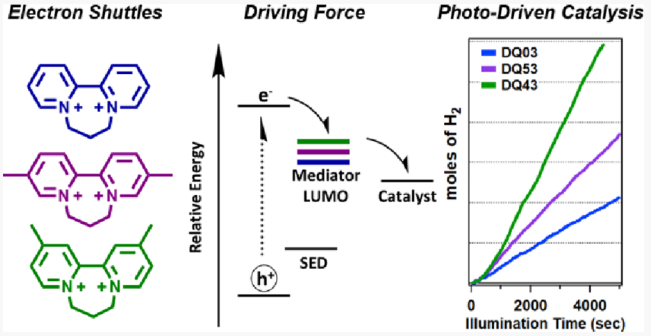

INTRODUCTION

Oxidoreductase enzymes, such as hydrogenase, carbon monoxide dehydrogenase (CODH), and nitrogenase, catalyze a variety of important chemical transformations with efficiency and selectivity rarely observed in manmade molecular catalysts under ambient conditions using earth-abundant transition metals.[1,2] Hence, this class of enzymes has been studied with the aim of reproducing these properties in artificial systems.[2−4] However, study of these systems presents several experimental challenges, in particular the complexity of initiating multi-electron and coupled proton transfer reactions to activate the stable small molecule substrates (H_2, CO_2, and N_2) as well as the stability and availability of the enzyme itself. Adding to these difficulties, many commonly studied oxidoreductase enzymes typically undergo hundreds up to thousands of turnovers per second, occupying intermediate states on the submillisecond timescale.[1,5,6] It is possible to observe the more stable intermediates by titrating them thermodynamically or under steady-state conditions.[7−10] However, often the most interesting intermediates are the more reactive and hence transient. It is for this reason that the application of traditional enzymology techniques for studying the catalytic mechanisms of many oxidoreductases is limited.[3] Techniques that can probe the sample on an appropriate timescale are needed due to the short lifetime of these intermediate populations but are currently underdeveloped.

To address this gap, several new approaches aimed at accessing these transient catalytic events have been developed recently. One such approach is the incorporation of nanocrystalline semiconductors (NCS) as a way to photoinitiate catalysis in the enzyme or molecular catalyst.[11−13] The NCS acts as a photosensitizer by absorbing light to create an exciton followed by electron transfer to the catalyst. This approach relies on direct electron injection from the NCS to an enzyme attached to its surface. Promising results have been obtained

Received: June 23, 2020
Revised: September 10, 2020
Published: September 14, 2020

https://dx.doi.org/10.1021/acs.jpcb.0c05718
J. Phys. Chem. B XXXX, XXX, XXX−XXX

with this approach, both in improving the lifetime of the enzyme relative to systems that use electrodes as the initiation method and in the mechanistic study of catalysts such as nitrogenase and hydrogenase.[11,12,14] Despite these breakthroughs, direct electron injection from the semiconductor to the enzyme is not a robust approach because of its low efficiency. Interfacial electron transfer (ET) is slow due to the long distances involved and the difficulty of controlling the enzyme orientation on the surface. Consequently, the ET efficiency is low due to competing parasitic processes such as radiative and non-radiative exciton decay as well as exciton-exciton annihilation.[15] These unproductive pathways result in short-lived excited states and present a hurdle for photodriven systems.[16,17] One way to circumvent this issue is to incorporate a redox mediator that can efficiently quench electrons from the semiconductor, and then deliver them to the biocatalyst before these parasitic events can occur.[18] Recently, we have developed and applied this mediated ET approach for rapidly injecting electrons into hydrogenases to initiate turnover (Figure 1A).[19]

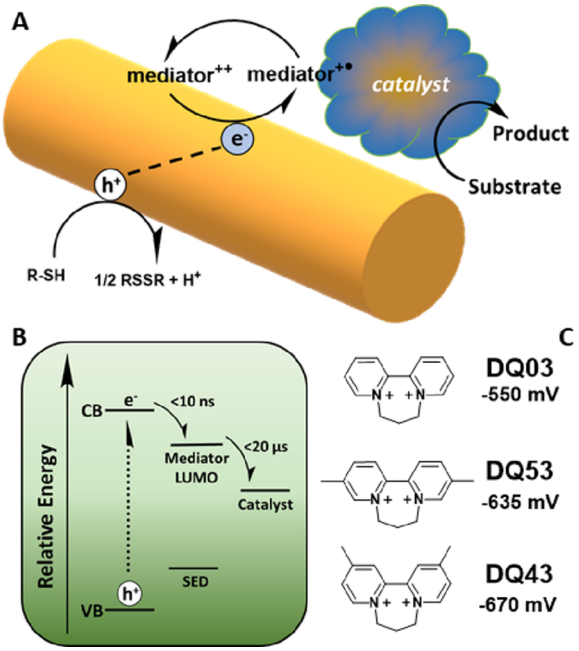

Figure 1. Components of the potential jump system. (A) Schematic of the overall ET pathway from the photosensitizer to mediator to enzyme catalyst to substrate. (B) Relative energy levels for each electron transfer step and component (VB = valence band; CB = conduction band; SED = sacrificial electron donor; LUMO = lowest unoccupied molecular orbital). (C) Mediators investigated in this work: DQ03, DQ53, and DQ43 with reduction potentials (vs NHE) listed beneath. The nomenclature of the mediators refers to the position of the methyl groups (0 = no methyl groups; 5 = methyl groups in the 5-position; 4 = methyl groups in the 4-position) and the number of carbons in the linker chain between the nitrogens (3 = 3-carbon chain).

This method has allowed us to monitor active site chemistry on a subturnover timescale and to improve the quantum efficiency for photodriven catalysis with an enzyme.[3,18,20,21] The initial photoinduced ET step in the photosensitizer-mediator pathway happens very fast (<10 ns) with near-unity quantum efficiency[18,22] and results in the accumulation of reducing equivalents in the form of one-electron reduced mediator. This accumulation leads to an extremely fast change in solution potential or a "potential jump". A potential jump induced by a short-pulsed laser can be used to trigger enzyme turnover via fast ET to the enzyme at timescales much shorter (typically 5−60 μs)[21] than the steady-state turnover frequency. This approach has been used successfully to study two of the three classes of hydrogenase enzymes, [NiFe] and [FeFe] hydrogenases, on subturnover timescales.[18−20,23−25] Previous application of this approach to study hydrogenase, however, raised questions about the details of this method.[18,20,21] Namely, what are the limits to efficiency and solution potential jump magnitude associated with different experimental conditions? How might the rate of ET change with the introduction of different conditions? Furthermore, systems such as CODH may require more negative solution potentials to achieve similar results or, in the case of nitrogenase, more reducing equivalents. To make this a viable approach for the study of such multi-electron oxidoreductases, bigger potential jumps, and more precise control of their magnitude are needed.

With the goal of optimizing the laser induced potential jump as a general method for the study of oxidoreductases, we screened several experimental conditions including pH, mediator concentration, protein concentration, photosensitizer concentration, and photon flux. We optimized conditions for the potential jump using an [FeFe] hydrogenase from *Chlamydomonas reinhardtii* (*Cr*HydA1) as our model oxidoreductase enzyme. *Cr*HydA1 is a convenient model system because of its extremely high turnover frequency (TOF), up to several thousands of turnovers per second.[26−28] The results of this study improve our understanding of the factors that control the potential jump within the context of the [FeFe] hydrogenase studied previously with this method as well as open the door to the application of this approach to study other enzymatic systems.

MATERIALS AND METHODS

Synthesis of Mediators (DQ03, DQ53, and DQ43). Mediators were synthesized using procedures modified from the literature.[29] Briefly, 5 mL of 1,3-dibromopropane and 0.25 g of 2,2′-bipyridine (5,5′-dimethyl-2,2′-bipyridine for DQ53 or 4,4′-dimethyl-2,2′-bipyridine for DQ43) were combined in a three-neck flask under inert atmospheric conditions. The reaction mixture was refluxed at 120−130 °C for 3−5 h at which point a pale yellow precipitate had formed within the flask. After the reaction ran to completion, the vessel was cooled in an ice bath and the solid collected on a frit. Excess reagents were washed from the product with cold acetone and hexane. The product was recrystallized from ethanol.

Synthesis of CdSe Seeds. This procedure is similar to the previously reported one.[18,21] Briefly, cadmium oxide (CdO) (0.06 g), trioctylphosphine oxide (TOPO) (3 g), and octadecylphosphonic acid (ODPA, purchased from Alpha Aesar) (0.28 g) were combined in a three-neck flask and put under vacuum while heating to 150 °C for 1.5 h. After this initial reaction period, the reaction vessel was put under a N_2 atmosphere. Once under N_2, the flask was heated to 350 °C until the reaction mixture became clear, indicating that the Cd had fully dissolved in the solvent. At this point, 1.5 mL of trioctylphosphine (TOP) was injected. After the reaction temperature recovered to about 340 °C, the Se precursor solution was injected. The Se precursor solution was prepared by dissolving 0.058 g of Se into 0.45 mL of trioctylphosphine (TOP). The reaction to produce nanocrystalline CdSe ran for

https://dx.doi.org/10.1021/acs.jpcb.0c05718
J. Phys. Chem. B XXXX, XXX, XXX−XXX

5 min, after which the vessel was removed from heat and cooled to room temperature. The particles were suspended in hexane and stored in the dark until needed.

Preparation of CdSe/CdS Dot-in-Rod (DIR). CdSe/CdS dot-in-rod (DIR) nanostructures were prepared by first synthesizing CdSe seeds and growing a CdS shell over the seeds. This was accomplished according to a modified literature procedure.[18] Briefly, CdO (0.06 g), TOPO (3 g), hexylphosphonic acid (HPA) (0.08 g), and ODPA (0.28 g) were combined in a three-neck flask and put under vacuum while heating to 150 °C for 2 h. After this initial period, the reaction vessel was placed under a N_2 atmosphere. Once under N_2, the flask was heated to 350 °C until the reaction mixture became clear, at which point 1.5 mL of trioctylphosphine (TOP) was injected. Once the reaction temperature recovered (to ≈340 °C), the sulfur precursor solution containing the CdSe seeds was injected. The sulfur precursor solution was prepared by dissolving sulfur (0.12 g) into TOP (1.5 mL) along with 2−3 mg of precipitated CdSe seeds. The reaction proceeded for 5 min. For slightly larger or smaller particles, the reaction time and temperature were adjusted accordingly.[30] Once the reaction was completed, the vessel was removed from heat and cooled to room temperature. A small volume of hexane or toluene was added to keep the reaction mixture in the solution phase. For use in aqueous media, the purified particles were solubilized through a ligand exchange reaction that has been described elsewhere to yield mercaptopropionic acid (MPA) capped DIR nanostructures.[18,20,21]

Preparation of *Cr*HydA1 [FeFe] Hydrogenase. *Cr*HydA1 apo-hydrogenase was produced recombinantly in *E. coli*, purified by Strep-tag affinity chromatography, and artificially maturated with the addition of $(Et_4N)_2[Fe_2(adt)(CO)_4(CN)_2]$ as described previously.[31,32]

Photodriven Mediator Reduction. Typical experimental conditions are listed here and are similar to those used by others.[18,21,33] Samples contained CdSe/CdS DIR nanoparticles (0.2−0.3 O.D. at 405 nm), 200 mM MPA sacrificial electron donor and mediator concentrations between 1 and 30 mM. The total volume for each sample was 1.4 mL in 50 mM sodium phosphate buffer and adjusted to the appropriate pH (between 6.5 and 10.5). Samples were prepared anaerobically inside of a glovebox under a 95% N_2 and 5% H_2 atmosphere. The cuvette was sealed with a rubber septum and Teflon tape, and inlet−outlet needles were inserted to allow a continuous flow of N_2 through the headspace of the cuvette to maintain an inert atmosphere.

Samples were illuminated with a 4.4 mW, 405 nm diode laser (Thor labs), and the absorbance was monitored with a fiber-optic coupled Ocean Optics UV−vis spectrometer (model QE65000). Samples were illuminated in 10 s intervals and allowed to equilibrate with the laser off for 10 s intervals while stirring continuously. QE is calculated by dividing moles of radical generated by moles of photons absorbed by the sample:

$$QE_{rad} = \frac{n_{med}}{\phi_q(1 - 10^{-A_{405}})t} \quad (1)$$

where n is moles of radical (mediator$^{\bullet+}$), calculated using Beer's law ($A = \varepsilon \times c \times l$); ϕ_q is the photon flux (photons per second) determined from the diode laser power; A_{405} is the DIR absorbance at 405 nm, and t is the illumination time. Full details of this calculation are presented in the Supporting Information.

Photodriven Hydrogen Production. The samples used for these experiments were also prepared anaerobically inside of a glovebox under a 95% N_2 and 5% H_2 atmosphere and performed similarly to the mediator reduction experiments except for the inclusion of 0.1 nmol hydrogenase. A Phidgets differential pressure sensor (part #: 1137_0) was inserted into the cap of the cuvette to monitor the change in pressure. This change in pressure was used to determine the amount of H_2 generated during the experiment using Henry's law.

Potential Jump Sample Preparation. Samples used for potential jump experiments were prepared anaerobically in the dark and were composed of 50 mM sodium phosphate buffer (pH 6.5, 7.5, or 8.5), 50 mM redox mediator, 200 mM MPA sacrificial electron donor, and CdSe/CdS nanorods with O.D. ≈ 0.3 at 355 nm as well as a *Cr*HydA1 enzyme concentration between 1 and 4 mM.

Simultaneous Transient Visible/Infrared Absorption Spectroscopy. Nanosecond transient absorbance was used to follow the generation of reduced mediator (DQ03$^{\bullet+}$, DQ53$^{\bullet+}$, or DQ43$^{\bullet+}$, 785 nm), its consumption by the enzyme, and the concomitant response of the enzyme active site H-cluster (CO absorbance near 5 μm). The instrument used to collect the infrared and visible transient absorbance (TA) data simultaneously has been described previously.[19] Briefly, the pump−probe experiment employs the third harmonic of a Q-switched Nd:YAG laser (10 ns pulse at 355 nm) as the pump pulse and two continuous wave probe lasers, a QCL operating in the mid-IR and a 785 nm diode laser. The time-resolved absorbance of the two probes as is detected using a fast MCT detector and an avalanche photodiode, respectively. Single shot transients were collected at room temperature using 100 μJ of 355 nm light focused to an ≈500 μm diameter spot (50 mJ/cm^2). An average of 20−25 shots was obtained for every probe wavelength. The transient absorbance signal was calculated as

$$\Delta A = -\log(I_{light}/I_{dark}) \quad (2)$$

where I_{dark} is the signal before the arrival of the pump pulse at time zero. From ΔA, the magnitude of the potential jump or the concentration of radical produced was calculated using Beer's law.

RESULTS AND DISCUSSION

System Components: Photosensitizer, Mediators, and Biocatalyst. System components employed in this study were chosen so that comparisons can be drawn between previously published results and those presented here.[18,20−22] A nanocrystalline semiconductor CdSe/CdS dot-in-rod (DIR) was used as our model photosensitizer for its previously established high quantum efficiency for ET to this class of mediator.[18] Upon photoexcitation of the DIR photosensitizer, an electron is promoted to the conduction band (CB) followed by ET to the mediator LUMO (Figure 1B). This ET step occurs with near-unity quantum efficiency[18] and results in a rapid (≈10 ns) potential jump as the solution potential becomes more negative by several hundred millivolts, triggering ET to the enzyme and enzyme turnover.

This study also surveys three different propyl-bridged 2,2′-bipyridinium salts (DQ03, DQ53, and DQ43) as electron carriers (Figure 1C). The utility of these mediators as electron

https://dx.doi.org/10.1021/acs.jpcb.0c05718
J. Phys. Chem. B XXXX, XXX, XXX−XXX

shuttles has been demonstrated previously,[20,29,34] but detailed analysis and quantification of their limitations under potential jump conditions remained in need of further exploration as only a few examples of these small molecules as electron shuttles exist in the literature. Like other viologens, these mediators have the advantage of forming long-lived and relatively stable radical species that can persist in solution for hundreds of microseconds up to minutes.[18,21] They also have more negative redox midpoint potentials (higher energy LUMOs) than other commonly used mediators, such as methyl viologen. A higher energy LUMO has the advantage of increasing the rate of forward electron transfer to the catalyst because of a greater driving force, ultimately resulting in a higher net efficiency of the system.

Steady-State Quantum Yield of Photodriven Mediator Reduction and Hydrogen Production. Steady-state photoillumination experiments were performed to determine the quantum efficiency of light-driven mediator reduction (QE_{rad}) as a function of mediator concentration and pH. Illumination of the CdSe/CdS DIR with blue light (405 nm) produces an exciton state, which the mediator quenches by extracting an electron from the conduction band (CB) of the DIR, generating a reduced mediator population (mediator$^{\bullet+}$). Representative absorbance spectra of the DQ03$^{\bullet+}$, DQ53$^{\bullet+}$, and DQ43$^{\bullet+}$ species as they are generated with sample illumination are shown in Figure S3. The absorbance feature at around 510 nm was monitored and used to determine the concentration of reduced mediator generated using Beer's law. QE_{rad} was calculated using eq 1 by dividing moles of radical generated by moles of photons absorbed.[18,21,33] The QE_{rad} is calculated from the first 10 s of illumination, before the concentration of mediator$^{\bullet+}$ builds up, thus minimizing contributions from back ET and other parasitic processes that lead to mediator degradation (full details of the calculation are presented in the Supporting Information). With this experiment, two key sets of conditions were compared, initial mediator concentration and pH, while consistently holding the concentration of photosensitizer to an optical density (OD) of 0.3 at 405 nm. This photosensitizer concentration was chosen to yield uniform excitation of the sample. An OD that is too high (greater than 0.6) leads to depletion of the pump laser and a transverse excitation gradient.

The starting concentration of the mediator is an important consideration, as use of too little can cause underperformance of the photosystem by leaving excited state electrons unquenched. On the other hand, a high starting mediator concentration relative to the concentration of nanoparticles in solution can lead to particle aggregation. The positively charged mediator associates electrostatically with the negatively charged carboxylate groups of the mercaptopropionic acid (MPA) capping ligands on the DIR. When a concentration of mediator sufficient to neutralize the surface of the particle is reached, the nanocrystals tend to aggregate in water. This has been observed with smaller particles, MPA capped CdSe QDs,[21] where the particles were observed to aggregate in solution when no enzyme was present and the mediator concentration was greater than 5 mM.

QE_{rad} was determined for all three mediators at four different concentrations: 1, 5, 10, and 30 mM (at pH 7.4), and the results are summarized in Figure 2A. For all three mediators, it was found that there was little benefit to having starting concentrations greater than 10 mM. Specifically, DQ03 already had a QE_{rad} of 80% at 1 mM while DQ53 and DQ43 gave lower QE_{rad} values (40% and 20%, respectively). Increasing the concentration of DQ03 to 10 mM gave a QE_{rad} of 95%, which could not be increased further. For DQ53, a concentration of 5 mM boosted the QE_{rad} to 65%, which increased slightly (to 70%) at 30 mM. For DQ43, increasing the mediator concentration gave a nonlinear increase in the QE_{rad} value up to 40% at 30 mM. The saturation behavior observed for each mediator is due to its binding to the surface of the DIR through an electrostatic interaction between the negatively charged capping ligands of the nanomaterial and the positively charged mediator, as described earlier. Previously, we had measured the binding efficiency of DQ03 to DIR photosensitizers and found it to have a K_d of ≈100 μM.[18] Accounting for multiple binding sites on the surface of the DIR puts saturation in the 1−10 mM range. Once this saturating concentration is reached, maximum exciton quenching efficiency is achieved.

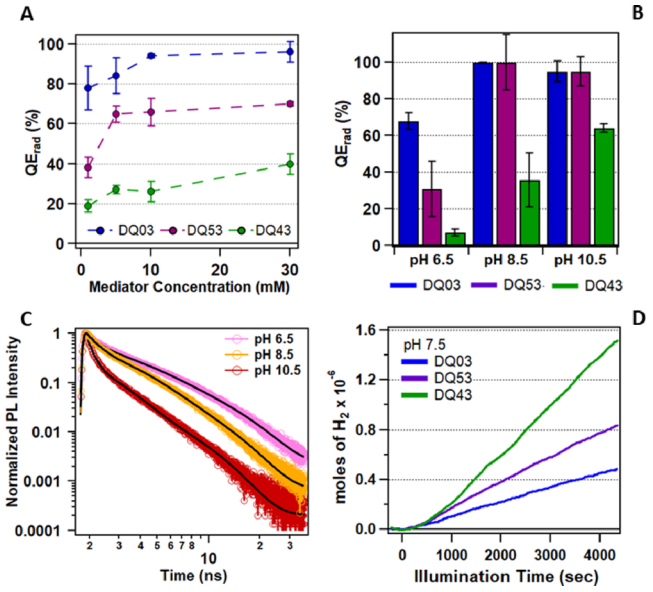

Figure 2. Steady-state mediator photoreduction and hydrogen production results. (A) Mediator reduction quantum efficiency (QE_{rad}) as a function of mediator starting concentration at pH 7.4. (B) QE_{rad} of mediator reduction versus pH with 25 mM mediator. (C) Time-dependent photoluminescence (PL) measured by time-correlated single photon counting, comparing hole transfer efficiency for different pH values (light pink = pH 6.5, orange = pH 8.5, maroon = pH 10.5). (D) Light-driven H_2 production assays with DIR-mediator-*Cr*HydA1 under optimized conditions at pH 7.5 with 25 mM mediator and 100 nM *Cr*HydA1 (blue = DQ03, purple = DQ53, and green = DQ43).

Another condition evaluated was the pH dependence of photodriven mediator reduction. One limitation of this class of photosensitizer is that the capping ligand frequently used for application in aqueous media (mercaptopropionic acid) participates in acid base chemistry. The end that is covalently attached to the surface of the particle, a thiol group, can be deprotonated to form thiolate with a pK_a between 6 and 7. The consequence of deprotonation is an increase in exciton lifetime in the DIR (*vide supra*), improving the overall ET efficiency to the mediator. The other end of the ligand, a carboxylate, can be protonated under acidic conditions. Protonation of the capping ligand neutralizes the DIR structure leading to aggregation and precipitation, setting the lower pH limit of around 6.

https://dx.doi.org/10.1021/acs.jpcb.0c05718
J. Phys. Chem. B XXXX, XXX, XXX−XXX

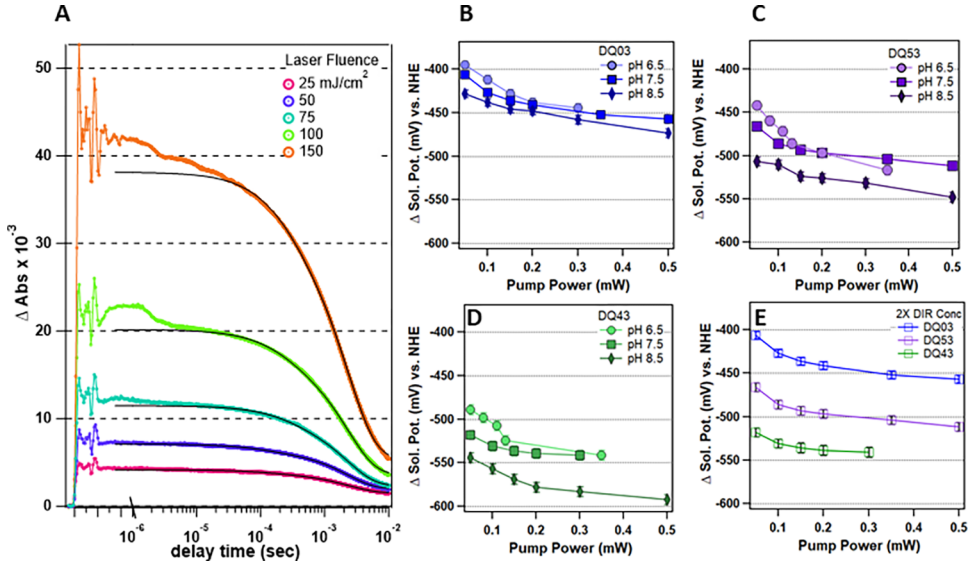

Figure 3. Representative transient absorbance data examining the pump power dependence under various conditions and how it relates to changes in solution potential. (A) Pump power dependence of radical transient absorbance following excitation with a 10 ns laser pulse for DQ53 at pH 8.5 (color scheme: magenta = 25 mJ/cm^2, blue = 50 mJ/cm^2, turquoise = 75 mJ/cm^2, light green = 100 mJ/cm^2, and orange = 150 mJ/cm^2). (B–D) Summary of pump power dependence data at different pH values for (B) DQ03, (C) DQ53, and (D) DQ43. (E) Summary of pump power dependence data at pH 7.5 for samples containing 2X the normal concentration of DIR. Symbols: circles = pH 6.5, squares = pH 7.5, diamonds = pH 8.5.

Photodriven mediator reduction was performed across a range of pH values (6.5, 8.5, and 10.5) to evaluate this dependency and its influence on QE_{rad} while maintaining the mediator concentration at 25 mM (Figure 2B). From this study, it was determined that more alkaline conditions led to greater observed QE_{rad} for mediator reduction. Specifically, DQ03 had a QE_{rad} of ≈60% at pH 6.5 while DQ53 and DQ43 gave lower QE_{rad} values (35% and 7%, respectively). Increasing the pH of the solution to pH 8.5 gave a QE_{rad} greater than 90%, for both DQ03 and DQ53. For DQ43, a solution pH of 8.5 increased the QE_{rad} to 37%. The QE_{rad} of DQ43 continued to improve slightly at even more basic conditions (to 60%).

We reasoned that this pH-dependent trend was likely related to pH-dependent hole transfer effects. Because the nanomaterial capping ligand MPA can act as a hole acceptor for the initial excitonic state, the hole transfer efficiency is affected by the charge of the capping ligand.[18,35] If the thiol group of the capping ligand is deprotonated (thiolate), more efficient hole transfer is expected compared to when it is protonated. The presence of hydroxide can also be a contributing factor as hydroxide has been shown to actively participate in hole scavenging.[36] More efficient hole scavenging reduces the parasitic process of back electron transfer, thereby increasing the efficiency of mediator reduction. Because hole filling quenches the photoluminescence (PL) of the nanomaterial, PL lifetimes are a direct probe of hole transfer rates.[37−39] We measured the PL lifetimes using time-correlated single photon counting in order to compare hole transfer efficiencies at different pH values (Figure 2C). As the pH was increased, faster hole transfer rates to the capping ligand were observed compared to acidic pH. The hole transfer lifetime for the DIR sample can be determined by fitting the change in PL intensity to a sum of exponential functions and calculating the amplitude weighted lifetime (AWL). The multi-exponential behavior of the PL intensity decay is partly due to the heterogeneity of the surface of the material, trap states, and localization of holes on the DIR surface. From this experiment, it was found that the DIR sample at pH 6.5 featured a hole transfer lifetime (τ = 3.24 ns) that was approximately seven times slower than for the sample at pH 10.5 (τ = 0.46 ns).

Finally, the mediators were compared for their efficacy as electron carriers to *Cr*HydA1 by the production of H_2 gas. This experiment was performed at pH 7.5 with 25 mM mediator and 100 nM *Cr*HydA1. Conditions were chosen to optimize the performance of the catalyst[40] (*Cr*HydA1) while balancing the efficiency of the DIR-mediator system. The amount of H_2 generated was determined by monitoring the change in pressure versus illumination time (Figure 2D) using a differential pressure sensor mounted in the cuvette cap. DQ43 gave the highest rate of 2.7 s^{-1} (molecules of H_2 produced per enzyme per second), three times higher than the poorest performing mediator, DQ03 (0.9 H_2 s^{-1}). When no enzyme was included in the photosystem, no change in pressure was observed (Figure S4), consistent with no production of H_2 in the absence of the catalyst as previously observed with similar mediator/nanocrystalline systems.[21]

We reasoned that the better performance of DQ43 as a mediator is due to the more negative solution potential generated by using a mediator that has a more negative redox midpoint potential, leading to an overall greater driving force for forward electron transfer to *Cr*HydA1. Indeed, by monitoring the UV–vis spectrum during the assay, we were able to quantify the amount of reduced mediator generated (Figure S4), which showed that DQ43 achieved a much more negative solution potential (−0.55 mV) than DQ53 and DQ03 (−0.48 and −0.42 mV respectively). We conclude that the significant difference in solution potential reached for each mediator, and so the driving force for enzyme reduction is responsible for the observed trend in hydrogen production.

In all cases, the observed rate of H_2 production was far less than the maximum turnover rate of up to several thousand per second measured for *Cr*HydA1 under similar conditions.[40]

https://dx.doi.org/10.1021/acs.jpcb.0c05718
J. Phys. Chem. B XXXX, XXX, XXX−XXX

Because the rate of mediator radical formation (ranging between 0.5 and 1.5 s^{-1}) is closely correlated with the rate of H_2 production, it is clear the rate of radical formation was the limiting factor in these experiments. The rate of production of reduced mediator is in turn limited by the fluence of the diode laser light source because the overall quantum yield of this process approaches unity. Thus, a higher laser fluence should yield a greater H_2 production rate, closer to what has been observed previously for this enzyme when the electron source is not limited.

Factors Affecting Potential Jump. The broad application of the laser induced potential jump technique to the study of oxidoreductase enzymes requires the elucidation of factors which tune its magnitude and lifetime. Like the approach taken in the steady-state experiments, a variety of conditions were surveyed: photon flux, photosensitizer concentration, mediator midpoint potential, and pH dependence. These factors were each found to contribute considerably to the magnitude of the jump and thus to the transient change in solution potential.

For this study, visible transient absorption (TA) spectroscopy was used to monitor the transient radical population. The production of reduced mediator and decay was monitored by probing the near IR absorbance band of the one electron reduced state of these mediators at 785 nm. Because the timescale of the transient measurements could potentially report on changes in the ground state of the DIR, a probe wavelength that does not overlap with any of the DIR absorbance bands is needed. So rather than using the feature around 510 nm as in the steady-state experiments, the 785 nm wavelength was used to probe the population of mediator$^{\bullet+}$ without potential convolution from transient features related to the DIR. A 510 nm probe is appropriate for steady-state experiments because it gives a better signal-to-noise ratio and is performed on a timescale too slow to capture any changes in absorbance related to the DIR. For these reasons, 785 nm is the more reliable probe to quantify the concentration of reducing equivalents generated in the time-resolved experiments. The samples were prepared anaerobically with a mediator concentration of 25 mM and DIR absorbance of 0.2 at 355 nm (except for samples containing 2X the amount of nanorods) to maintain consistent photon absorption between samples. The first condition evaluated was the laser fluence. The range of laser fluence explored spanned 25 mJ per cm^2 to 150 mJ per cm^2 for each mediator at pH 6.5, 7.5, or 8.5. A representative data set is presented in Figure 3A. The 785 nm absorption signal due to mediator radical formation rises with an instrument limited lifetime of <10 ns. The concentration of radical produced varied between 100 μM and 10 mM depending on pump power and sample conditions. From the change in absorbance (ΔA) at 1 μs, the concentration of reduced mediator and the solution potential were calculated using Beer's law and the Nernst equation (full details of these calculations are presented in the Supporting Information).[20,41,42]

Consistent with observations made in the steady-state photodriven mediator reduction experiments, the greatest jumps were observed at pH values greater than 7. For example, the DQ03 sample showed an initial formation of 0.1 mM radical at the greatest pump power for pH 6.5, but 0.4 mM radical was achieved at pH 8.5. This corresponds to a solution potential ≈30 mV more negative at pH 8.5 than at pH 6.5 (Figure 3B). DQ53 and DQ43 followed a similar pattern, though because of their more negative reduction potentials, larger jumps were observed. For example, at pH 6.5 the largest jump observed for DQ53 (Figure 3C) had a solution potential of −505 mV, but at pH 8.5, the largest pump power resulted in a solution potential 45 mV more negative. DQ43 (Figure 3D) continued this trend with a jump ≈35 mV more negative at pH 8.5 than at pH 6.5.

When the concentration of DIR was doubled, greater jumps were observed under the same pH conditions (Figure 3E), leading to increases in the radical concentration at the greatest pump power. These results of the pump power and pH dependence are summarized in Table S4 in the Supporting Information.

It is worth noting that greater than 80% of the radical signal formed decays by ≈5 ms in these TA experiments despite the absence of an electron acceptor (e.g., hydrogenase or other catalyst). This decay occurs consistently with a half-life of ≈2 ms for all three mediators. The similarity in decay rates indicates an effect that is intrinsic to the mediator radical itself and is not influenced by pH. We attribute this decay to the formation of what is described as a "pimer" state or the π-stacking of two one-electron reduced mediators (Figure 4).[43,44]

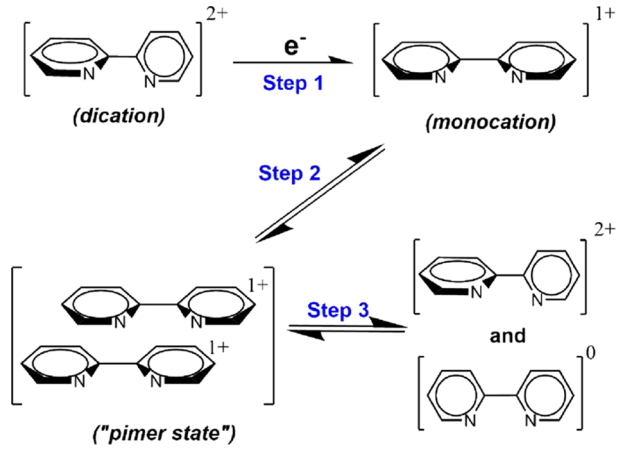

Figure 4. Schematic describing the pimer formation process. Upon one-electron reduction of the dication mediator (step 1) to form the monocation species, a change in orientation of the two pyridine rings results in a more planar configuration of the mediator. This planar configuration allows for the formation of the "pimer state" (step 2) and from which disproportionation can occur (step 3). (Bridging carbons and methyl groups have been omitted from this scheme for clarity.)

Upon reduction, bipyridinium molecules undergo a change in conformation from a twisted state to a more planar configuration (step 1) allowing π-stacking to occur and the pimer state to form (step 2). Once formed, the pimer state will readily undergo disproportionation to form the doubly reduced mediator and reform the dication in solution (step 3).[45,46] The decay observed is due to the disappearance of the mediator$^{\bullet+}$ in favor of the formation of mediator^{++} and mediator^{0}. It has been reported that the formation of the pimer state causes a small redshift in the near IR absorbance band, which may also contribute to the observed decay.

The doubly reduced mediator^{0} is insoluble in water and therefore not likely to be an effective electron carrier. We were unable to identify a spectroscopic signature for this state, so we do not know how long it persists in solution following the disproportionation reaction. Furthermore, the TR-IR measurements (Figure 5) indicate that the doubly reduced mediator^{0}

https://dx.doi.org/10.1021/acs.jpcb.0c05718
J. Phys. Chem. B XXXX, XXX, XXX−XXX

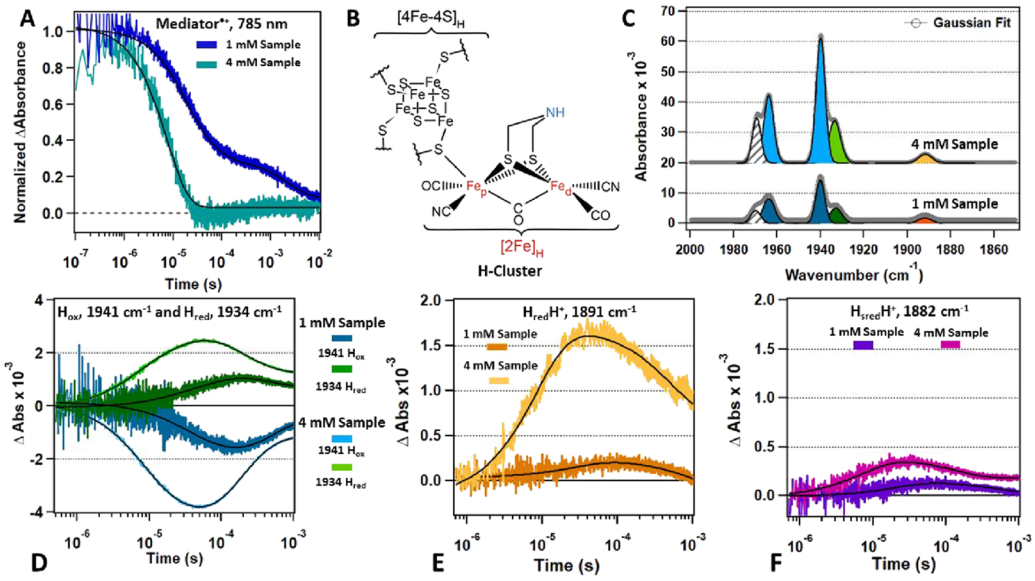

Figure 5. Time-resolved Visible (TR-Vis) and IR (TR-IR) measurements with samples containing 1 or 4 mM *Cr*HydA1 at pH 7.4 in the presence of CdSe/CdS DIR and 25 mM DQ03. (A) TR-Vis traces of DQ03 at 785 nm for 1 mM (blue) and 4 mM (turquoise) samples. (B) Structure of the active site (H-cluster) of *Cr*HydA1 [FeFe] hydrogenase. (C) FTIR of both 1 and 4 mM *Cr*HydA1 containing samples used for transient absorbance measurements. The 4 mM sample has been offset for clarity. Intermediate populations are colored as follows: blue = H_{ox}; green = H_{red}; orange = $H_{red}H^+$; gray striped = H_{ox}-CO. (D) TR-IR traces of *Cr*HydA1 in the H_{ox} (1941 cm^{-1}, blue) and H_{red} (1934 cm^{-1}, green) states for 1 mM (dark) and 4 mM (light) enzyme samples. (E) TR-IR traces of the $H_{red}H^+$ state (1891 cm^{-1}) in 1 mM (orange) and 4 mM (yellow) samples. (F) TR-IR traces of the $H_{sred}H^+$ state (1882 cm^{-1}) in 1 mM (purple) and 4 mM (magenta) samples.

produced in the slow disproportionation process does not reduce the enzyme (no enzyme reduction occurs on this timescale). We conclude that the process of pimer disproportionation is an unproductive pathway that limits the potential jump to the millisecond timescale. Nevertheless, the radical population persists long enough to drive catalysis in the case of hydrogenase. If the reaction of reduced mediator with the target enzyme is slow (on the ms timescale), then this radical decay pathway will greatly reduce the efficiency of the system. This is observed even in hydrogenase experiments when a low enzyme concentration is used.[20] For other enzymes, the ET might be intrinsically slow (not diffusion limited) and therefore inherently inefficient due to this parasitic pathway.

Kinetics of ET to *Cr*HydA1 Hydrogenase. A laser-induced potential jump coupled with transient absorbance (TA) in the visible and infrared were used to follow the kinetics of ET from mediator to *Cr*HydA1 and subsequent formation of intermediate states on a subturnover timescale, respectively. Two potential jump samples containing *Cr*HydA1 were prepared with differing enzyme concentrations (1 and 4 mM) at pH 7.4 and 25 mM DQ03 mediator. These enzyme concentrations were chosen to examine the effect on the kinetics of varying the ratio of reducing equivalents to protein. The radical concentration generated in the potential jump is held constant in these experiments, yielding a ratio of reducing equivalents:enzyme of approximately 1:2 for the 1 mM sample and 1:8 for the 4 mM sample. Although DQ03 did not perform as well as DQ43 for light-driven H_2 production, we chose DQ03 for these experiments to directly compare performance to results previously obtained with *Cr*HydA1 and CdSe/CdS NRs.[20] The radical population was monitored in the same way as in the previous TA experiments, when no enzyme was present, by probing at 785 nm. Additionally, intermediate populations were monitored in the infrared to determine if there is a difference in population flux through different intermediate states when exposed to varying concentrations of radical.

The population of mediator radical was monitored by TA at 785 nm (Figure 5A), showing significant differences in decay of the radical signal for the 1 and 4 mM samples. For the lower enzyme concentration (1 mM), three kinetics phases were observed (Figure 5A), with lifetimes of 15 μs, 60 μs, and 2.2 ms. There are three possible radical decay pathways: charge recombination (CR), ET to enzyme (ET), and pimer disproportionation (PD). The three lifetimes observed for the 1 mM enzyme sample correspond to these three pathways; the same 15 μs and 2.2 ms phases are observed in control experiments without the enzyme (Figure 3A); therefore, we assign them to the CR and PD processes, respectively. The intermediate phase (τ = 60 μs) represents ET to the enzyme. The fastest kinetics phase may also have some contribution from ET to the enzyme based on the TR-IR data (Figure 5). Although there is an excess of enzyme present, some radical still decays by the PD pathway with its characteristic lifetime of 2.2 ms. We postulate that pimer formation is fast and competitive with the ET pathway under these conditions and that its decay rate is determined by the rate of disproportionation. All three radical decay pathways are bimolecular (they require mediator:rod, mediator:enzyme, or mediator:mediator collisions, respectively) and thus should be concentration-dependent up to a point of saturation.[20] When the *Cr*HydA1 enzyme concentration is increased to 4 mM, the radical population decayed monoexponentially to zero with a 20 μs lifetime. With the increased enzyme concentration, the ET pathway is as fast as the CR pathway; therefore, only a single exponential decay is observed. Furthermore, the PD pathway is no longer observed in this case, likely because pimer formation is no longer competitive with ET.

https://dx.doi.org/10.1021/acs.jpcb.0c05718
J. Phys. Chem. B XXXX, XXX, XXX−XXX

The populations of multiple intermediate states of the active site (H-cluster) in the [FeFe] hydrogenase were also monitored to determine the influence of the magnitude of this first reduction step on intermediate population dynamics (Figure 5). The H-cluster is composed of a canonical [4Fe-4S] cluster attached to a unique [2Fe] cluster containing two terminal CO and two terminal CN^- ligands, a bridging CO ligand, and a bridging 2-azapropane 1,3-dithiolate ligand (Figure 5B).[28] The CO and CN^- ligands have vibrational frequencies in a mid-IR region free of protein absorbance (1800−2200 cm^{-1}). The vibrational frequencies of the CO ligands are particularly sensitive to the oxidation and protonation states of the H-cluster, and so the distribution of catalytic intermediates can be followed by tuning in to a specific CO frequency (Figure 5C). The CO peaks are easily monitored by TA methods because of their relatively large extinction coefficients and because there are often multiple frequencies assigned to an intermediate, aiding the selection of a frequency that reports on a single intermediate population.

Under mildly oxidizing conditions (in the absence of H_2), the H-cluster is in the active oxidized state H_{ox} with the most intense IR band at ≈1941 cm^{-1}. One-electron reduction yields two different reduced states, commonly called H_{red} and $H_{red}H^+$. H_{red} is thought to have most of the extra electron density located on the [4Fe-4S] cluster site, resulting in only small (5−10 cm^{-1}) redshifts to the IR bands. Hence, the most intense IR band of the H_{red} state is observed at ≈1934 cm^{-1}. The $H_{red}H^+$ state is thought to have the electron density shifted more onto the [2Fe] site giving much larger (20−60 cm^{-1}) shifts in the IR bands. The most intense peak for $H_{red}H^+$ is, therefore, observed at 1891 cm^{-1}. Finally, one-electron reduction of the [4Fe-4S] cluster in the $H_{red}H^+$ state gives the $H_{sred}H^+$ state with a major band at 1882 cm^{-1}. Here, we followed the transition from H_{ox} to H_{red} and $H_{red}H^+$ as well as the transition to form $H_{sred}H^+$ in *Cr*HydA1.

The rates of depletion and formation of the H_{ox} and H_{red} intermediate populations were calculated from the values obtained by fitting the transient data to a sum of exponential functions (details and final fitting coefficients are summarized in the Supporting Information). The bleach of the H_{ox} feature at 1941 cm^{-1} (Figure 5D) corresponds to the one electron reduction of the H-cluster to give H_{red} and $H_{red}H^+$. Both the 1 and 4 mM *Cr*HydA1 containing samples featured biexponential decays of their H_{ox} populations. For instance, the 1 mM sample had H_{ox} decay rates of 28 and 90 μs while the 4 mM sample had H_{ox} decay rates of 7 and 35 μs. Similar biexponential reduction of *Cr*HydA1 has been observed before and was attributed to two different pathways through the protein for ET to the active site.[20] This interpretation is further supported by the biexponential rate of formation of the H_{red} intermediate (Figure 5D). Both the 1 and 4 mM samples feature two formation constants that closely match the two decay lifetimes of the H_{ox} population, 20 and 94 μs for the 1 mM sample and 5 and 24 μs for the 4 mM sample. The biexponential behavior is not observed with the formation of $H_{red}H^+$ (Figure 5E) intermediates however, though its formation also matched the faster rate of H_{ox} decay with lifetimes of 29 and 9 μs for the 1 and 4 mM samples, respectively. Interestingly, very little formation of the two-electron intermediate, $H_{sred}H^+$, was observed in these experiments, suggesting that, even at the lower enzyme concentration, predominantly a single-electron transfer to the enzyme occurs. Production of a small population of $H_{sred}H^+$ monitored at 1882 cm^{-1} (Figure 5F) is likely the result of one-electron reduction of the H_{red} population that is present at the beginning of the experiment (Figure 5B). Its formation rate (8 μs) is similar to the rate of formation of the one-electron intermediates, H_{red} and $H_{red}H^+$. Since the H_{red} and $H_{red}H^+$ states form on very similar timescales, proton transfer to the H-cluster must be on the same timescale or faster than electron transfer from the mediator to the enzyme.

CONCLUSIONS

Previously, we established the viability of a method of shuttling electrons to a catalyst via viologen-based mediators in the context of a mechanistic study of a specific enzyme (hydrogenase), though the general utility of the approach not yet been well established.[18,21] Also lacking from the previous work was careful measurement of the timescale and magnitude of the laser induced potential jump, characteristics necessary to determine the applicability of this technique for study of other systems. In the work presented here, several parameters were screened to address these unresolved questions as well as to provide the framework for the application of this system for the study of other biocatalysts, including pH, mediator midpoint potential and concentration, photosensitizer concentration, protein concentration, and photon flux.

First, in steady-state measurements, it was observed that the QE_{rad} of electron quenching by the mediator is quite sensitive to pH and mediator concentration. These observations are due to hole transfer effects and surface coverage by the mediator, respectively, and indicate that careful tuning of these two conditions can maximize the quantum efficiency of photo-driven catalysis with oxidoreductases. In kinetic studies, it was found that the magnitude of the jump varied with sample conditions as observed in the steady-state experiments. The expected correlation between laser power and radical production allows tuning of the magnitude of the potential jump simply by increasing the pump power. At the highest pump power tested, the solution potential was lowered by several hundred millivolts in response to the laser pulse. Despite having the poorest QE_{rad} in steady-state measurements, DQ43 produced the largest change in solution potential, achieving a final solution potential of −600 mV under one set of conditions. The change in solution potential is generated within the time of the laser pulse (10 ns in the present work), which is fast enough to observe flux through intermediate states of very fast catalysts like hydrogenase. In addition, the potential jump is sufficiently negative to permit the study of previously inaccessible catalytic events in enzymes such as CODH that require highly reducing conditions to drive catalysis. Also, the magnitude of the jumps achieved in the experiments presented here does not represent the upper limit of jumps attainable. Based on these results, even larger jumps could be expected by varying some of the conditions explored, such as using higher concentrations of the photosensitizer. The ability to achieve a large potential jump allows for the exploration of both one and two ET processes and to compare their rates since multi-electron catalysts often require increasingly negative reduction potentials for subsequent reductions (i.e., the catalyst gets harder to reduce after the first ET).

The lifetime of the potential jump is another important characteristic for establishing its applicability to fast enzyme reactions. The risetime of the potential jump in our

https://dx.doi.org/10.1021/acs.jpcb.0c05718
J. Phys. Chem. B XXXX, XXX, XXX−XXX

experiments was limited by the laser pulsewidth of 10 ns, although we have previously shown that ET from the photosensitizer to the mediator occurs on the picosecond timescale. Diffusion of the mediator and ET to the enzyme will clearly be rate-limiting in most cases. The rate of ET to the hydrogenase enzyme was manipulated (increased or decreased) by altering the protein concentration. Increasing the concentration from 1 to 4 mM resulted in a doubling of the rate of radical consumption, indicating that this first ET step is at least partially diffusion-controlled. The persistence of the potential jump is limited by the phenomenon of pimer formation and disproportionation, which causes the radical population to decay on the millisecond timescale. Though not ideal, this decay does not hinder study of fast oxidoreductases, provided that ET to the enzyme occurs before this decay on the millisecond timescale.

Finally, the optimum mediator for driving a specific enzyme reaction depends on both the midpoint potential of the enzyme and its turnover frequency. For example, when two different hydrogenases (one [NiFe] and the other [FeFe]) with approximately the same midpoint potentials are compared in the same photodriven system, a significant difference in the optimum mediator for light-driven H_2 production becomes apparent. We have shown previously that [NiFe] SHI from *Pyrococcus furiosus* had the highest turnover rate when paired with the DQ53 mediator,[21] and the rate of H_2 production decreased when the more negative redox mediator DQ43 was used. In contrast, the *Cr*HydA1 [FeFe] hydrogenase used in the present study performed best when paired with the most negative redox mediator, DQ43. We reasoned that this is due to the approximately 100 times slower turnover rate of [NiFe] hydrogenase relative to *Cr*HydA1. The greater driving force of ET from the more negative mediator DQ43 accelerates parasitic charge recombination (CR) such that it becomes competitive with ET to the [NiFe] hydrogenase. The faster turnover rate of *Cr*HydA1 allows it to outcompete CR with DQ43, resulting in more efficient overall performance. This example highlights the need for careful matching of the enzyme turnover frequency and the driving force of the ET from the mediator to the enzyme to maximize efficiency of this process.

Cumulatively, these results lay the foundation for the application and expansion of this technique to enable the study of other biocatalytic systems, such as CODH or nitrogenase. In principle, they also demonstrate the potential for the substitution of other mediators or photosensitizers to tailor this approach for the desired study.

■ ASSOCIATED CONTENT

Supporting Information

The Supporting Information is available free of charge at https://pubs.acs.org/doi/10.1021/acs.jpcb.0c05718.

> Material characterization, quantum efficiency of photodriven mediator reduction, steady-state solution potential during hydrogen production, fit coefficients for TCSPC data, data analysis for TR-Vis measurements, analysis of laser induced potential jump; fit coefficients for TR-Vis and TR-IR data, and proposed catalytic cycle for [FeFe] hydrogenase (PDF)

■ AUTHOR INFORMATION

Corresponding Authors

James A. Birrell − *Max Planck Institute for Chemical Energy Conversion, Mülheim an der Ruhr 45470, Germany;* orcid.org/0000-0002-0939-0573; Email: James.birrell@cec.mpg.de

R. Brian Dyer − *Department of Chemistry, Emory University, Atlanta, Georgia 30030, United States;* orcid.org/0000-0002-0090-7580; Email: briandyer@emory.edu

Authors

Monica L. K. Sanchez − *Department of Chemistry, Emory University, Atlanta, Georgia 30030, United States*

Sara E. Konecny − *Department of Chemistry, Emory University, Atlanta, Georgia 30030, United States*

Sarah M. Narehood − *Department of Chemistry, Emory University, Atlanta, Georgia 30030, United States*

Edward J. Reijerse − *Max Planck Institute for Chemical Energy Conversion, Mülheim an der Ruhr 45470, Germany;* orcid.org/0000-0001-9605-4510

Wolfgang Lubitz − *Max Planck Institute for Chemical Energy Conversion, Mülheim an der Ruhr 45470, Germany;* orcid.org/0000-0001-7059-5327

Complete contact information is available at: https://pubs.acs.org/10.1021/acs.jpcb.0c05718

Notes

The authors declare no competing financial interest.

■ ACKNOWLEDGMENTS

This work was supported by the National Science Foundation grants CHE1807865 and DMR1808288 (to R.B.D.). J.A.B., E.R., and W.L. were funded by the Max Planck Society. J.A.B. acknowledges funding from the Deutsche Forschungsgemeinschaft (DFG) Priority Programme "Iron-Sulfur for Life: Cooperative Function of Iron-Sulfur Centers in Assembly, Biosynthesis, Catalysis and Disease" (SPP 1927) Project BI 2198/1-1. The authors thank Nina Breuer for help preparing *Cr*HydA1.

■ ABBREVIATIONS

CB, conduction band; CR, charge recombination; Cr, *Chlamydomonas reinhardtii*; DIR, dot-in-rod; ET, electron transfer; LUMO, lowest unoccupied molecular orbital; MPA, mercaptoproprionic acid; NCS, nanocrystalline semiconductor; PD, pimer disproportionation; PL, photoluminescence; QE, quantum efficiency; TA, transient absorbance; TR-IR, time-resolved infrared; TOPO, trioctylphosphine oxide; VB, valence band

■ REFERENCES

(1) Cai, R.; Minteer, S. D. Nitrogenase Bioelectrocatalysis: From Understanding Electron-Transfer Mechanisms to Energy Applications. *ACS Eng. Lett.* **2018**, *3*, 2736−2742.

(2) Evans, R. M.; Siritanaratkul, B.; Megarity, C. F.; Pandey, K.; Esterle, T. F.; Badiani, S.; Armstrong, F. A. The Value of Enzymes in Solar Fuels Research − Efficient Electrocatalysts through Evolution. *Chem. Soc. Rev.* **2019**, *48*, 2039−2052.

(3) Greene, B. L.; Schut, G. J.; Adams, M. W. W.; Dyer, R. B. Pre-Steady-State Kinetics of Catalytic Intermediates of an [FeFe]-Hydrogenase. *ACS Catal.* **2017**, *7*, 2145−2150.

(4) Woolerton, T. W.; Sheard, S.; Chaudhary, Y. S.; Armstrong, F. A. Enzymes and Bio-Inspired Electrocatalysts in Solar Fuel Devices. *Eng. Env. Sci.* **2012**, *5*, 7470−7490.
(5) Banerjee, R.; Jones, J. C.; Lipscomb, J. D. Soluble Methane Monooxygenase. *Annu. Rev. Biochem.* **2019**, *88*, 409−431.
(6) Wang, V. C. C.; Maji, S.; Chen, P. P. Y.; Lee, H. K.; Yu, S. S. F.; Chan, S. I. Alkane Oxidation: Methane Monooxygenases, Related Enzymes, and Their Biomimetics. *Chem. Rev.* **2017**, *117*, 8574−8621.
(7) Sommer, C.; Adamska-Venkatesh, A.; Pawlak, K.; Birrell, J. A.; Rüdiger, O.; Reijerse, E. J.; Lubitz, W. Proton Coupled Electronic Rearrangement within the H-Cluster as an Essential Step in the Catalytic Cycle of [FeFe] Hydrogenases. *J. Am. Chem. Soc.* **2017**, *139*, 1440−1443.
(8) Rodríguez-Maciá, P.; Pawlak, K.; Rüdiger, O.; Reijerse, E. J.; Lubitz, W.; Birrell, J. A. Intercluster Redox Coupling Influences Protonation at the H-cluster in [FeFe] Hydrogenases. *J. Am. Chem. Soc.* **2017**, *139*, 15122−15134.
(9) Senger, M.; Mebs, S.; Duan, J.; Shulenina, O.; Laun, K.; Kertess, L.; Wittkamp, F.; Apfel, U.-P.; Happe, T.; Winkler, M.; et al. Protonation/Reduction Dynamics at the [4Fe-4S] Cluster of the Hydrogen-Forming Cofactor in [FeFe]-Hydrogenases. *Phys. Chem. Chem. Phys.* **2018**, *20*, 3128−3140.
(10) Ratzloff, M. W.; Artz, J. H.; Mulder, D. W.; Collins, R. T.; Furtak, T. E.; King, P. W. CO-Bridged H-Cluster Intermediates in the Catalytic Mechanism of [FeFe]-Hydrogenase CaI. *J. Am. Chem. Soc.* **2018**, *140*, 7623−7628.
(11) Brown, K. A.; Harris, D. F.; Wilker, M. B.; Rasmussen, A.; Khadka, N.; Hamby, H.; Keable, S.; Dukovic, G.; Peters, J. W.; Seefeldt, L. C.; et al. Light-driven dinitrogen reduction catalyzed by a CdS:nitrogenase MoFe protein biohybrid. *Science* **2016**, *352*, 448.
(12) Brown, K. A.; Wilker, M. B.; Boehm, M.; Hamby, H.; Dukovic, G.; King, P. W. Photocatalytic Regeneration of Nicotinamide Cofactors by Quantum Dot−Enzyme Biohybrid Complexes. *ACS Catal.* **2016**, *6*, 2201−2204.
(13) Brown, K. A.; Dayal, S.; Ai, X.; Rumbles, G.; King, P. W. Controlled Assembly of Hydrogenase-CdTe Nanocrystal Hybrids for Solar Hydrogen Production. *J. Am. Chem. Soc.* **2010**, *132*, 9672−9680.
(14) Ratzloff, M. W.; Wilker, M. B.; Mulder, D. W.; Lubner, C. E.; Hamby, H.; Brown, K. A.; Dukovic, G.; King, P. W. Activation Thermodynamics and H/D Kinetic Isotope Effect of the H_{ox} to $H_{red}H^+$ Transition in [FeFe] Hydrogenase. *J. Am. Chem. Soc.* **2017**, *139*, 12879−12882.
(15) Utterback, J. K.; Wilker, M. B.; Mulder, D. W.; King, P. W.; Eaves, J. D.; Dukovic, G. Quantum Efficiency of Charge Transfer Competing against Nonexponential Processes: The Case of Electron Transfer from CdS Nanorods to Hydrogenase. *J. Phys. Chem. C* **2019**, *123*, 886−896.
(16) Wilker, M. B.; Shinopoulos, K. E.; Brown, K. A.; Mulder, D. W.; King, P. W.; Dukovic, G. Electron Transfer Kinetics in CdS Nanorod−[FeFe]-Hydrogenase Complexes and Implications for Photochemical H_2 Generation. *J. Am. Chem. Soc.* **2014**, *136*, 4316−4324.
(17) Brown, K. A.; Wilker, M. B.; Boehm, M.; Dukovic, G.; King, P. W. Characterization of Photochemical Processes for H_2 Production by CdS Nanorod−[FeFe] Hydrogenase Complexes. *J. Am. Chem. Soc.* **2012**, *134*, 5627−5636.
(18) Chica, B.; Wu, C.-H.; Liu, Y.; Adams, M. W. W.; Lian, T.; Dyer, R. B. Balancing Electron Transfer Rate and Driving Force for Efficient Photocatalytic Hydrogen Production In CdSe/CdS Nanorod−[NiFe] Hydrogenase Assemblies. *Energy Environ. Sci.* **2017**, *10*, 2245−2255.
(19) Greene, B. L.; Vansuch, G. E.; Chica, B. C.; Adams, M. W. W.; Dyer, R. B. Applications of Photogating and Time Resolved Spectroscopy to Mechanistic Studies of Hydrogenases. *Acc. Chem. Res.* **2017**, *50*, 2718−2726.
(20) Sanchez, M. L. K.; Wu, C.-H.; Adams, M. W. W.; Dyer, R. B. Optimizing Electron Transfer from CdSe QDs to Hydrogenase for Photocatalytic H_2 Production. *Chem. Commun.* **2019**, *55*, 5579−5582.
(21) Sanchez, M. L. K.; Sommer, C.; Reijerse, E.; Birrell, J. A.; Lubitz, W.; Dyer, R. B. Investigating the Kinetic Competency of CrHydA1 [FeFe] Hydrogenase Intermediate States via Time-Resolved Infrared Spectroscopy. *J. Am. Chem. Soc.* **2019**, *141*, 16064−16070.
(22) Zhao, F.; Li, Q.; Han, K.; Lian, T. Mechanism of Efficient Viologen Radical Generation by Ultrafast Electron Transfer from CdS Quantum Dots. *J. Phys. Chem. C* **2018**, *122*, 17136−17142.
(23) Greene, B. L.; Wu, C.-H.; Vansuch, G. E.; Adams, M. W. W.; Dyer, R. B. Proton Inventory and Dynamics in the Nia-S to Nia-C Transition of a [NiFe] Hydrogenase. *Biochemistry* **2016**, *55*, 1813−1825.
(24) Greene, B. L.; Wu, C.-H.; McTernan, P. M.; Adams, M. W. W.; Dyer, R. B. Proton-Coupled Electron Transfer Dynamics in the Catalytic Mechanism of a [NiFe]-Hydrogenase. *J. Am. Chem. Soc.* **2015**, *137*, 4558−4566.
(25) Greene, B. L.; Joseph, C. A.; Maroney, M. J.; Dyer, R. B. Direct Evidence of Active-Site Reduction and Photodriven Catalysis in Sensitized Hydrogenase Assemblies. *J. Am. Chem. Soc.* **2012**, *134*, 11108−11111.
(26) Sickerman, N. S.; Hu, Y. Hydrogenases. *Methods Mol. Biol.* **2019**, *1876*, 65−88.
(27) Wittkamp, F.; Senger, M.; Stripp, S. T.; Apfel, U. P. [FeFe]-Hydrogenases: recent developments and future perspectives. *Chem. Commun.* **2018**, *54*, 5934−5942.
(28) Lubitz, W.; Ogata, H.; Rüdiger, O.; Reijerse, E. Hydrogenases. *Chem. Rev.* **2014**, *114*, 4081−4148.
(29) Xiao, Y.; Chu, L.; Sanakis, Y.; Liu, P. Revisiting the IspH Catalytic System in the Deoxyxylulose Phosphate Pathway: Achieving High Activity. *J. Am. Chem. Soc.* **2009**, *131*, 9931−9933.
(30) Wu, K.; Hill, L. J.; Chen, J.; McBride, J. R.; Pavlopolous, N. G.; Richey, N. E.; Pyun, J.; Lian, T. Universal Length Dependence of Rod-to-Seed Exciton Localization Efficiency in Type I and Quasi-Type II CdSe@CdS Nanorods. *ACS Nano* **2015**, *9*, 4591−4599.
(31) Berggren, G.; Adamska, A.; Lambertz, C.; Simmons, T. R.; Esselborn, J.; Atta, M.; Gambarelli, S.; Mouesca, J. M.; Reijerse, E.; Lubitz, W.; et al. Biomimetic assembly and activation of [FeFe]-hydrogenases. *Nature* **2013**, *499*, 66.
(32) Esselborn, J.; Lambertz, C.; Adamska-Venkatesh, A.; Simmons, T.; Berggren, G.; Noth, J.; Siebel, J.; Hemschemeier, A.; Artero, V.; Reijerse, E.; et al. Spontaneous Activation of [FeFe]-Hydrogenases by an Inorganic [2Fe] Active Site Mimic. *Nat. Chem. Biol.* **2013**, *9*, 607−609.
(33) Zhu, H.; Song, N.; Lv, H.; Hill, C. L.; Lian, T. Near Unity Quantum Yield of Light-Driven Redox Mediator Reduction and Efficient H_2 Generation Using Colloidal Nanorod Heterostructures. *J. Am. Chem. Soc.* **2012**, *134*, 11701−11708.
(34) Kung, J. W.; Baumann, S.; von Bergen, M.; Müller, M.; Hagedoorn, P.-L.; Hagen, W. R.; Boll, M. Reversible Biological Birch Reduction at an Extremely Low Redox Potential. *J. Am. Chem. Soc.* **2010**, *132*, 9850−9856.
(35) Liang, Y.; Thorne, J. E.; Parkinson, B. A. Controlling the Electronic Coupling between CdSe Quantum Dots and Thiol Capping Ligands via pH and Ligand Selection. *Langmuir* **2012**, *28*, 11072−11077.
(36) Kamat, P. V.; Jin, S. Semiconductor Photocatalysis: "Tell Us the Complete Story!". *ACS Eng. Lett.* **2018**, *3*, 622−623.
(37) Song, N.; Zhu, H.; Jin, S.; Lian, T. Hole Transfer from Single Quantum Dots. *ACS Nano* **2011**, *5*, 8750−8759.
(38) Wu, K.; Du, Y.; Tang, H.; Chen, Z.; Lian, T. Efficient Extraction of Trapped Holes from Colloidal CdS Nanorods. *J. Am. Chem. Soc.* **2015**, *137*, 10224−10230.
(39) Thompson, C. M.; Kodaimati, M.; Westmoreland, D.; Calzada, R.; Weiss, E. A. Electrostatic Control of Excitonic Energies and Dynamics in a CdS Quantum Dot through Reversible Protonation of Its Ligands. *J. Phys. Chem. Lett.* **2016**, *7*, 3954−3960.
(40) Siebel, J. F.; Adamska-Venkatesh, A.; Weber, K.; Rumpel, S.; Reijerse, E.; Lubitz, W. Hybrid [FeFe]-Hydrogenases with Modified Active Sites Show Remarkable Residual Enzymatic Activity. *Biochemistry* **2015**, *54*, 1474−1483.

https://dx.doi.org/10.1021/acs.jpcb.0c05718
J. Phys. Chem. B XXXX, XXX, XXX−XXX

(41) Braterman, P. S.; Song, J. I. Spectroelectrochemistry of aromatic ligands and their derivatives. 1. Reduction products of 4,4′-bipyridine, 2,2′-bipyridine, 2,2′-bipyrimidine, and some quaternized derivatives. *J. Org. Chem.* **1991**, *56*, 4678−4682.
(42) Anderson, R. F.; Patel, K. B. Radical cations of some low-potential viologen compounds. Reduction potentials and electron-transfer reactions. *J. Chem. Soc., Faraday Trans. 1* **1984**, *80*, 2693−2702.
(43) Kertesz, M. Pancake Bonding: An Unusual Pi-Stacking Interaction. *Chem. − Eur. J.* **2019**, *25*, 400−416.
(44) Suzuki, S.; Morita, Y.; Fukui, K.; Sato, K.; Shiomi, D.; Takui, T.; Nakasuji, K. Aromaticity on the Pancake-Bonded Dimer of Neutral Phenalenyl Radical as Studied by MS and NMR Spectroscopies and NICS Analysis. *J. Am. Chem. Soc.* **2006**, *128*, 2530−2531.
(45) Lü, J.-M.; Rosokha, S. V.; Kochi, J. K. Stable (Long-Bonded) Dimers via the Quantitative Self-Association of Different Cationic, Anionic, and Uncharged π-Radicals: Structures, Energetics, and Optical Transitions. *J. Am. Chem. Soc.* **2003**, *125*, 12161−12171.
(46) Geraskina, M. R.; Dutton, A. S.; Juetten, M. J.; Wood, S. A.; Winter, A. H. The Viologen Cation Radical Pimer: A Case of Dispersion-Driven Bonding. *Am. Ethnol.* **2017**, *129*, 9563−9567.

https://dx.doi.org/10.1021/acs.jpcb.0c05718
J. Phys. Chem. B XXXX, XXX, XXX−XXX